



A multi-site kinetic model for NH₃-SCR over Cu/SSZ-13

Louise Olsson ^{a,*}, Kurnia Wijayanti ^a, Kirsten Leistner ^a, Ashok Kumar ^b, Saurabh Y. Joshi ^b, Krishna Kamasamudram ^b, Neal W. Currier ^b, Aleksey Yezerets ^b

^a Chemical Engineering, Competence Centre for Catalysis, Chalmers University of Technology, SE-412 96 Göteborg, Sweden

^b Cummins Inc., 1900 McKinley Avenue, MC 50183, Columbus, IN 47201, USA

ARTICLE INFO

Article history:

Received 18 December 2014

Received in revised form 21 February 2015

Accepted 27 February 2015

Available online 28 February 2015

Keywords:

Kinetic model

Multi-site

Ammonia-SCR

Cu/SSZ-13

Cu/zeolites

ABSTRACT

In this study, we have developed a kinetic model for ammonia-SCR over a well-characterized Cu/SSZ-13 catalyst. It was found that a three-site model was needed in order to describe the ammonia temperature programmed desorption (TPD) with adsorption at 50 and 150 °C as well as ammonia oxidation, and NH₃-SCR up to 600 °C. Based on literature studies, where detailed characterization of Cu/SSZ-13 have been conducted using several experimental techniques, we suggest the following physical interpretation of the S1 and S2 sites in the model. The S1 sites are associated with copper located in a six-membered ring, possibly slightly distorted due to interactions with water and ammonia while, the S2 sites represent copper in the large cages or Cu_xO_y species. In addition, ammonia is also stored on Brønsted acid sites, but in order not to complicate the model further, it was lumped together in the S1 and S2 sites. Finally, S3 sites have been added in order to describe the large amount of physisorbed ammonia at low temperature. This three-site model was capable of adequately describing the ammonia TPD experiments with the initial temperature of 50 and 150 °C. The heats of adsorption of ammonia on the S1 and S2 sites were determined using micro-calorimeter experiments. Further, the main SCR reaction in the model occurs on S1 sites and the main ammonia oxidation reaction on S2 sites. However, due to the complex behavior associated with ammonia oxidation, where the conversion slightly decreased when the temperature was increased from 350 to 400 °C, an ammonia oxidation reaction occurring at low temperature with low rate needed to be introduced on S1. In a similar way, an added step was needed for ammonia-SCR on S2, which occurred at high temperature where the ammonia coverage on S1 was low resulting in low conversion. To summarize, the three-site model developed was capable of well describing the ammonia storage and release, ammonia oxidation as well as SCR and N₂O formation across a broad temperature interval (100–600 °C).

© 2015 Elsevier B.V. All rights reserved.

1. Introduction

Selective catalytic reduction (SCR) using NH₃ as a reductant is a method for reducing NO_x in excess oxygen environments and is a widely used NO_x after treatment technology for diesel and lean-burn vehicles. Vanadia supported on titania [1–5] and Cu [6–14] and Fe-exchanged [15–17] zeolites have been extensively studied for this reaction. A major advantage of Cu/zeolites is that they exhibit a high level of activity at low temperature [18]. In the past few years, copper-zeolites and silicoaluminophosphate with chabazite (CHA) structure, like Cu/SAPo-34 [19] and Cu/SSZ-13 [20,21], have shown promising results because of their high hydro-thermal stability and hydrocarbon resistance [20].

The copper loading and location of Cu sites in zeolite framework play an important role in the activity of the Cu/zeolites. This finding has been observed for both model Cu/BEA [22] and Cu/SSZ-13 [23], and it was found that the rates for ammonia oxidation and NO oxidation are higher on over-exchanged Cu sites, whereas the opposite results were seen for standard SCR [22]. The framework for Cu/SSZ-13 consists of six-membered rings connected to form a cavity that is bounded by six 8-membered and twelve 4-membered rings [24]. There have been several studies devoted to understand the interactions between Cu sites and the zeolite framework by using catalysts with various copper loadings. In order to maximize the NO_x conversion over the range of operating conditions, Kwak et al. [25] found an optimal copper loading for Cu/SSZ-13 of about 40–60%. It was suggested by several authors [26–28] that copper is preferentially positioned in isolated positions in the six-membered rings for lower copper loadings. However, when water and ammonia are present in the feed mixture, copper moves slightly into the

* Corresponding author. Tel.: +46 31 772 4390; fax: +46 31 772 3035.

E-mail address: louise.olsson@chalmers.se (L. Olsson).

Nomenclature

A_i	Pre-exponential factor for reaction i (s^{-1})
d_{hyd}	Hydraulic diameter of the channel (m)
$E_{A,i}$	Activation energy for reaction i (J/mol)
$E_{A,i}^0$	Activation energy for reaction i at zero coverage (J/mol)
GSA	Geometric surface area per reactor volume (m^{-1})
$k_{k,m}$	Mass transfer coefficient of species k (mol/m ² s)
k_i	Rate constant for reaction i (s^{-1})
$MG_{K,G}$	Molar mass of gas phase species k (kg/kmol)
r_i	Reaction rate for reaction i (kmol/(s m ²))
T_s	Temperature at catalyst surface (K)
t	Time (s)
v_g	Gas velocity (m/s)
$v_{i,k}$	Stoichiometric coefficient of species k in reaction i (–)
$w_{k,g}$	Mass fraction of species k in gas phase (–)
y_{k}^B	Mole fraction at the reaction layer of specie k (–)
y	Mole fraction in the gas bulk of specie k (–)
z	Spatial coordinate in axial direction (m)

Greek letters

α_i	Coverage dependence in reaction i (–)
ϵ_g	Volume fraction of gas phase in entire system (–)
θ_k	Coverage of species k (–)
ρ_g	Density of the gas phase (kmol/m ³)
Ω_j	Surface site density of storage site j (kmol/m ²)

larger cages [29]. This observation is in line with the results found by Deka et al. [26], where based on XAFS and XRD data, it was proposed that interactions with ammonia at lower temperatures (125 °C) resulted in conformational change (from a square planar to a distorted tetrahedral type) and this change in coordination geometry was reversible at higher temperatures. For higher copper loadings, it is possible that copper is also located inside the large cage [29,30]. For Cu/SSZ-13 with Si/Al ratio of about 4.3–4.5, Bates et al. [28] suggested that when the Cu/Al is above 0.2, Cu_xO_y are also present. In addition, the Ribeiro research group observed that the NO oxidation rate started from zero at 0.2 Cu/Al and thereafter increased with copper loading [23]. Interestingly, Gao et al. [29] observed two regimes, below and above 250 °C with different activation energies for ammonia oxidation over Cu/SSZ-13, and suggested that this may be attributable to a change in the rate limiting mechanism or a change in the coordination of the Cu/ion catalytic centers resulting in different reactivity.

There are several kinetic models available in the literature for different ammonia-SCR catalysts, like vanadia on titania [1–5], Cu/ZSM-5 [31–34], Cu/faujasite [35], Cu/Beta [36], Cu/CHA [37], HZSM-5 [38] and Fe/zeolites [15–17,39]. For Cu/zeolites, both detailed [32–34] and global kinetic models [13,31,40] have been developed. The ammonia-SCR mechanism contains several important steps, where the first step often entails the adsorption of ammonia. The adsorption and desorption of ammonia are included in a kinetic model in order to describe transient effects and are crucial to the model. Wilken et al. [41] developed a method to determine the coverage dependent heat of adsorption at atmospheric pressure for ammonia on Cu/BEA which was directly used in a kinetic model [36]. This method resulted in linearly decreasing the heat of adsorption when increasing the ammonia coverage, which is in line with the Temkin isotherm. Both single site [31,36] kinetic models and multiple site [17,33,42,43] models have been developed for ammonia storage over zeolites. A reason for using multiple sites is to describe storage at low temperature, where large amount

of physisorbed ammonia is present [33]. In order to describe the selectivity of the SCR reaction at high temperatures, it is critical to include ammonia oxidation in the kinetic model [33,36]. For the standard SCR reaction [31,37,44], a stoichiometric reaction between NO and ammonia was used for Cu/zeolites, whereas for Fe/zeolites an overconsumption of ammonia, attributed to parasitic oxidation, was observed [45]. Another important reaction to consider in the kinetic models is the N₂O formation. We have previously developed an N₂O model for copper-zeolites capable of describing the maximum N₂O production occurring at low temperature and the simultaneous increase in N₂O at high temperature [36]. The reversible formation of ammonium nitrate species was crucial for the low temperature N₂O production, a reaction step that was also included in the study by Colombo et al. [44].

However, to our knowledge, there are no multi-site kinetic models available for NH₃-SCR over well-characterized Cu/zeolites with CHA structure, such as Cu/SSZ-13 and Cu/SAPO-34. The objective of this study is to develop a kinetic model for ammonia-SCR over a Cu/SSZ-13 model catalyst by combining flow reactor data and micro-calorimetry experiments over a broad temperature interval. In order to describe the ammonia storage and release in a broad temperature interval and in addition the activity of the catalyst from 100 to 600 °C, it was crucial to use a multi-site model.

2. Experimental

2.1. Catalyst preparation

Based on the method described by McEwen et al. [24], we have synthesized SSZ-13. In the first step, a 200 ml solution of 1 M NaOH was prepared by mixing NaOH (Sigma–Aldrich, >98% anhydrous pellets, S5881-1KG) with milliQ water and stirring the mixture for approx. 15 min. Thereafter, 320 g of milliQ water and 250 g of sodium silicate solution (Sigma–Aldrich 338443-1L) were added to the NaOH solution and the mixture was stirred for an additional 15 min. This procedure was followed by adding zeolite Y (Zeolyst International CBV300) spoon by spoon and the mixture was then agitated for 30 min. Finally, 105 g of a TMAAI solution (25% solution of tricyclo[3.3.1.13,7]decan-1-aminium,N,N,N-trimethyl-, hydroxide, from Sachem, ZeoGen SDA 2825) was added and the mixture stirred for another 30 min. The prepared mixture was transferred to a Teflon-lined, stirred autoclave, heated to 140 °C and left in this condition for six days (including the time to heat it up from room temperature). Thereafter, the autoclave was cooled to room temperature. Most of the liquid was decanted, the remaining solid/liquid mixture was washed with milliQ water, separated by vacuum filtration and then left to dry at room temperature. The powder obtained was calcined for 8 h at 550 °C, with a ramp of 0.5 °C/min (17 h, 40 min for the ramp).

The prepared SSZ-13 was transformed into an ammonium form by treating it with 0.25 M NH₄NO₃ (99%, Sigma–Aldrich), using a ratio of volume of solution (mL) to weight of zeolite (g) of 7:1. The powder was slowly added to the solution and the pH was adjusted to about 3–3.5 using diluted NH₄OH. Thereafter, the temperature was increased to 80 °C and the solution continuously stirred for 75 min, during which the pH was maintained in the 3–3.5 interval using diluted NH₄OH. After the ion exchange, the sample was cooled and the liquid removed. A day later, the powder was washed seven times with milliQ water and dried in an oven at 90 °C for 12 h. This procedure was followed by ion-exchanging the zeolite three times with a 250 ml 0.025 M Cu(NO₃)₂ (98%, Alfa Aesar GmbH) solution. The solution was heated to 80 °C and at this temperature, the powder was slowly added and the solution thereafter kept at this temperature under stirring for 75 min. The resulting powder was washed seven times with milliQ water until a neutral pH was

received. Finally, the powder was dried for 12 h at 90 °C and calcined in the air at 600 °C for 4 h with a ramping rate of 5 °C min⁻¹.

The powder was washcoated on a 400 cpsi monolith, with the dimensions 2 cm in length and 2.1 cm in diameter. A detailed description of the procedure for washcoating can be found in Wijayanti et al. [46]. In order to improve the attachment of the zeolite layer, a thin alumina layer was first applied (67 mg), which was followed by zeolite coating (780 mg), including 5% boehmite as a binder. The prepared monolith was calcined in an oven at 600 °C for 2 h.

2.2. Catalyst characterization

The structure of the zeolite was examined using XRD. The X-ray diffractograms were obtained by using a BrukerAXS D8 advance operating at 40 kV and 40 mA with nickel-filtered Cu K α radiation ($\lambda = 1.5418 \text{ \AA}$) in the range of $5^\circ < 2\theta < 40^\circ$ with a step size of 0.029. The surface area and pore volume was detected with N₂ physisorption at -195°C using a Micromeritics ASAP 2010 instrument after degassing the powder under vacuum at 240°C for 3 h. An elemental analysis was conducted using an inductively coupled plasma sector field mass spectrometry (ICP-SFMS).

2.3. Micro-calorimeter experiments

In order to measure the heat of adsorption of ammonia, micro-calorimeter experiments were conducted using a Setaram Sensys equipment. The experimental setup has been described in earlier publications [41,46]. The catalyst powder (50 mg) was placed on a sintered quarts plate inside a quarts reactor. The sample is exposed to different gases at atmospheric pressure using Bronkhorst mass flow controllers, with a total flow of 20 ml/min and Ar as inert balance. The gases were analyzed using a Hidden HPR-20 QUI mass spectrometer (MS). First, the catalyst was pretreated using 8% O₂ at 500°C for 20 min to clean its surface. Thereafter, the temperature was set to 500°C , while exposing the catalyst to Ar only. At 500°C , the catalyst was exposed to 1000 ppm NH₃ for 150 min in order to adsorb the most strongly bound ammonia. This step was followed by decreasing the temperature to 450°C using Ar only as feed gas, and when the desired temperature was reached, the sample was again exposed to 1000 ppm ammonia for 150 min. This procedure was repeated for 400, 350, 300, 250, 200, 150, 100 and finally at 50°C , using an exposure time for NH₃ of 180 min.

2.4. Flow reactor experiments

A flow reactor was used to measure the activity and selectivity and this system is described in more detail in [46]. Briefly, the gases were mixed using multiple mass-flow controllers and the gas received was flown over the monolith catalyst, which was placed in a horizontal quarts tube. The temperature was measured and regulated using a thermocouple placed in the gas phase before the catalyst. In addition, the temperature was measured with a second thermocouple placed inside a center channel. The gases were analyzed using an MKS Multigas 2030 FTIR spectrometer that monitored the concentrations of NH₃, NO, NO₂, N₂O, as well as H₂O. A total flow of 3500 ml min^{-1} was used, resulting in a space velocity of $30,300 \text{ h}^{-1}$, and argon was used as the inert balance in all experimental sequences.

Initially, the catalyst was degreened using 400 ppm NO, 400 ppm NH₃, 8% O₂ and 5% H₂O for 4 h at 650°C . Thereafter, the catalyst was pre-treated in order to clean the surface by exposing it to 8% O₂ and 5% H₂O at 600°C for 20 min. This pre-treatment was conducted prior to all experiments, in order to have a clean surface when starting each experiment. Two ammonia temperature programmed (TPD) experiments were conducted, one with adsorption

at 50°C and another at 150°C , using 400 ppm NH₃ and 5% H₂O for 90 min. Thereafter, the catalyst was flushed with 5% H₂O in Ar for 80 min, followed by increasing the temperature to 600°C using a ramp speed of $10^\circ\text{C}/\text{min}$. The ammonia oxidation was examined by exposing the catalyst to 400 ppm NH₃, 8% O₂ and 5% H₂O and increasing the temperature stepwise from 150 to 600°C . The SCR activity was studied in a similar experiment using 400 ppm NH₃, 400 ppm NO, 8% O₂ and 5% H₂O, and increasing the temperature in steps from 100 to 600°C . Finally, experiments were conducted with a focus on the low conversion regime for the purpose of performing Arrhenius plots both for ammonia oxidation and ammonia-SCR, using the same gas mixture as described above in the temperature range of 200 – 290 and 70 – 150°C , respectively.

3. Kinetic modeling

3.1. Reactor model

The kinetic modeling was performed with a commercial software, AVL BOOST, version 2013 [47], using one channel model. The channel was discretized in an axial direction using 20 grid points and the mass-transfer in the washcoat was simulated using five grid points.

The main governing equation for the gas phase species is:

$$\epsilon_g \frac{\partial \rho_g \times w_{k,g}}{\partial t} = \epsilon_g \frac{\partial \rho_g \times w_{k,g} \times v_g}{\partial z} + MG_{k,g} \sum_i^{nr} v_{i,k} \times r_i (y_k, T_s, \theta_k) \quad (1)$$

and for the coverage of component k on the surface:

$$\frac{\partial \theta_k}{\partial t} (\Theta \times \text{GSA}) = \sum_i^{nr} v_{i,k} \times r_i (y_k, T_s, \theta_k) \quad (2)$$

where the geometric surface area per unit reactor volume, GSA, is given by:

$$\frac{\text{GSA}}{d_{\text{hyd}}} = 4 \times (\text{celldensity}) \quad (3)$$

Mass-transfer, both in the gas phase and the washcoat were simulated. The film model was used to describe the external mass transport from the gas bulk to the surface, using the following equation:

$$\text{GSA} \times k_{k,m} \times (y_k - y_k^B) = \sum_i^{nr} v_{i,k} \times r_i (y_k, T_s, \theta_k) \quad (4)$$

For the mass-transfer in the washcoat a constant pore diffusion model was applied using effective diffusivity of the different gas components of $5 \times 10^{-6} \text{ m}^2/\text{s}$, according to Chatterjee et al. [48].

The heat balance was not solved because of the low heat of reaction for the SCR reactions in combination with the low concentration of the reacting species. This approach was used in several previous models [6,17,31–34,36]. In the simulations, the temperature measured in the catalyst was used.

3.2. Kinetic model

The rate constants are described using the Arrhenius equation, according to

$$k_i = A_i e^{-E_{A,i}/(RT_s)} \quad (5)$$

Ammonia storage and release is a crucial function for the transient operation of an SCR catalyst, especially for zeolite containing materials since they store very large quantities [7,18,20,49]. We

Table 1
Reactions and rate expressions.

Reaction	Reaction rate	Reaction number
$\text{NH}_3 + \text{S1} \xrightleftharpoons{r_1} \text{S1} - \text{NH}_3$	$r_{1f} = \Psi_{\text{S1}} k_{1,f} y_{\text{NH}_3} \theta_{\text{S1}}$ $r_{1b} = \Psi_{\text{S1}} k_{1,b} \theta_{\text{S1}-\text{NH}_3}$	(1)
$\text{NH}_3 + \text{S2} \xrightleftharpoons{r_2} \text{S2} - \text{NH}_3$	$r_{2f} = \Psi_{\text{S2}} k_{2,f} y_{\text{NH}_3} \theta_{\text{S2}}$ $r_{2b} = \Psi_{\text{S2}} k_{2,b} \theta_{\text{S2}-\text{NH}_3}$	(2)
$\text{NH}_3 + \text{S3} \xrightleftharpoons{r_3} \text{S3} - \text{NH}_3$	$r_{3f} = \Psi_{\text{S3}} k_{3,f} y_{\text{NH}_3} \theta_{\text{S3}}$ $r_{3b} = \Psi_{\text{S3}} k_{3,b} \theta_{\text{S3}-\text{NH}_3}$	(3)
$2\text{S1} - \text{NH}_3 + 1.5\text{O}_2 \xrightleftharpoons{r_4} \text{N}_2 + 3\text{H}_2\text{O} + 2\text{S1}$	$r_4 = \Psi_{\text{S1}} k_4 y_{\text{O}_2}^{0.6} \theta_{\text{S1}-\text{NH}_3}$	(4)
$2\text{S2} - \text{NH}_3 + 1.5\text{O}_2 \xrightleftharpoons{r_5} \text{N}_2 + 3\text{H}_2\text{O} + 2\text{S2}$	$r_5 = \Psi_{\text{S2}} k_5 y_{\text{O}_2}^{0.6} \theta_{\text{S2}-\text{NH}_3}$	(5)
$4\text{S1} - \text{NH}_3 + 4\text{NO} + \text{O}_2 \xrightleftharpoons{r_6} 4\text{N}_2 + 6\text{H}_2\text{O} + 4\text{S1}$	$r_6 = \Psi_{\text{S1}} k_6 y_{\text{NO}} y_{\text{O}_2}^{0.5} \theta_{\text{S1}-\text{NH}_3}$	(6)
$4\text{S2} - \text{NH}_3 + 4\text{NO} + \text{O}_2 \xrightleftharpoons{r_7} 4\text{N}_2 + 6\text{H}_2\text{O} + 4\text{S2}$	$r_7 = \Psi_{\text{S2}} k_7 y_{\text{NO}} y_{\text{O}_2}^{0.5} \theta_{\text{S2}-\text{NH}_3}$	(7)
$\text{S2} - \text{NH}_3 + \text{NO} \xrightleftharpoons{r_8} \text{S2} - \text{NH}_3 - \text{NO}$	$r_{8f} = \Psi_{\text{S2}} k_{8,f} y_{\text{NO}} \theta_{\text{S2}-\text{NH}_3}$ $r_{8b} = \Psi_{\text{S2}} k_{8,b} \theta_{\text{S2}-\text{NH}_3-\text{NO}}$	(8)
$2\text{S2} - \text{NH}_3 - \text{NO} + \text{O}_2 \xrightleftharpoons{r_9} \text{N}_2\text{O} + \text{N}_2 + 3\text{H}_2\text{O} + 2\text{S2}$	$r_9 = \Psi_{\text{S2}} k_9 y_{\text{O}_2} \theta_{\text{S2}-\text{NH}_3-\text{NO}}$	(9)
$2\text{S2} - \text{NH}_3 + 2\text{NO} + \text{O}_2 \xrightleftharpoons{r_{10}} \text{N}_2\text{O} + \text{N}_2 + 3\text{H}_2\text{O} + 2\text{S2}$	$r_{10} = \Psi_{\text{S2}} k_{10} y_{\text{O}_2} y_{\text{NO}} \theta_{\text{S2}-\text{NH}_3}$	(10)

previously developed a method for measuring the coverage dependent heat of adsorption of ammonia on Cu/zeolites at atmospheric pressure [41]. When increasing the coverage, this method resulted in a linear decrease in ΔH which is in line with the Temkin isotherm. It is often assumed that the adsorption is non-activated [50]; thus, the activation energy for ammonia desorption can be described using the Temkin isotherm as follows:

$$E_{A,i} = E_{A,i}^0 (1 - \alpha_i \times \theta_{\text{S1}-\text{NH}_3}) \quad (6)$$

Temkin isotherms have been used in many kinetic models to describe the ammonia desorption [5,16,31,33,51].

All reactions and rates used in the final model are shown in Table 1, with the corresponding parameters in Table 2. Note that these parameters are the final values, however several other parameters have been used in the model development and the values and results of these will also be shown and discussed in Section 4. The model is developed in successive steps and, therefore, the motivation for the different reaction steps will be discussed in Section 4. It should be noted that the activation energy for ammonia desorption from S1 is coverage dependent, according to Eq. (6), and the value given in the table is for zero coverage and the coverage dependent constant is shown in the foot note. For S2 and S3 sites constant values were used for the activation energy for desorption, because coverage dependence were not crucial for these sites. In this work, we have focused on SCR experiments that includes NO, which is the reason for that reaction steps for fast and NO_2 SCR is not added. Further, the NO oxidation activity for this catalyst was low, and we only receive 20–25 ppm NO_2 at 500–600 °C when exposing the catalyst to 400 ppm NO, 8% O_2 and 5% H_2O (results not shown here). In a DRIFT study by Sjövall et al. [7] using Cu/ZSM-5

it was found that the coverage of nitrites/nitrates decreased due to ammonia inhibition. Thus, it is likely that ammonia also inhibits the NO oxidation, which would result in even lower NO oxidation in SCR conditions. This in combination with the low NO oxidation activity was the reason for not adding NO oxidation to this model.

Initially, a single site model was investigated, but it did not capture the experimental features adequately, and this will be discussed thoroughly in Section 4. Over both Cu/BEA [22] and Cu/SSZ-13 [23], it has been suggested that the oxidation and SCR reactions occur on different types of copper species and it is therefore, important to include two active sites in the model. In addition, at low temperature large amount of physisorbed ammonia is observed and this can be modeled using a separate site, which was done by Sjövall et al. [33] for ammonia SCR over Cu/ZSM-5. In the final model presented in this paper three sites were used; denoted S1, S2 and S3. The physical interpretation of these sites is:

- S1: the main storage site. This site includes both copper and Brønsted acid sites, but in order not to further complicate the model, it is simulated as one site, using global reactions, something that has been successfully done in many previous studies [12,31,36,44,52,53]. The catalyst that is used in this study is under-exchanged and we therefore propose that the copper contributing to the S1 site is located in the six-membered ring, since for Cu/SSZ-13, copper is believed to be initially ion-exchanged into isolated positions in the six-membered rings [26–28].
- S2: site where ammonia is stored at high temperature. Ammonia storage has been observed at high temperature over pure H/SSZ-13 [54,55] and therefore, in the same way as for S1, this site is likely a combination of both ammonia stored on Brønsted sites as

Table 2
Parameters for the kinetic model for ammonia storage and release, ammonia oxidation, ammonia-SCR and N_2O formation.

Reaction	Pre-exp. factor, forward reaction (s^{-1})	Activation energy, forward reaction (kJ/mol)	Pre-exp. factor, backward reaction (s^{-1})	Activation energy, backward reaction (kJ/mol)
1. NH_3 ads./desorption, S1	1.21×10^4	0.0	10^{13}	149.0 ^{a,b}
2. NH_3 ads./desorption, S2	2.47×10^6	0.0	10^{13}	137.8 ^b
3. NH_3 ads./desorption, S3	10.6	0.0	2.04	18.6
4. NH_3 oxidation, S1 ^c	8.61×10^3	72.7 ^c	–	–
5. NH_3 oxidation, S2	1.79×10^{12}	195.0	–	–
6. NH_3 -SCR, S1 ^c	4.83×10^8	68.3 ^c	–	–
7. NH_3 -SCR, S2	1.67×10^{11}	105.0	–	–
8. $\text{S2}-\text{NH}_3-\text{NO}$ form./decomp.	3.30×10^7	63.0	2.68×10^{16}	145.0
9. N_2O formation from $\text{S2}-\text{NH}_3-\text{NO}$	2.49×10^7	35.0	–	–
10. High temp. N_2O formation	1.72×10^{11}	112.0	–	–

^a $\alpha=0.20$.

^b Determined from micro-calorimetry.

^c Determined from Arrhenius plots.

well as copper sites and in the model this was lumped together in the S2 site. However, some of the ammonia adsorbed at high temperature is likely associated with copper active sites in order to produce SCR activity at high temperature. Indeed, Mihai et al. [22] observed an increase in ammonia adsorbed at high temperature when increasing the copper loading in Cu/BEA. According to Gao et al. [29] and Kwak et al. [30], the copper present at higher copper loadings are occupying sites in the large cages. We therefore propose that the copper contributing to S2 sites are associated with copper in the large cages.

- S3: Site for loosely bound physisorbed ammonia. This ammonia can be physisorbed for example on copper, acid sites or sodium residues.

The physical interpretation and motivation of sites will be further discussed in Section 4.3.

4. Results and discussion

4.1. Catalyst characterization

The XRD measurements (results not shown here) of the powder zeolite sample confirmed the structure of the SSZ-13. The zeolite structure remained intact after the ion-exchange to form Cu/SSZ-13. The BET surface area was $439 \text{ m}^2/\text{g}$ and the total pore volume $0.22 \text{ cm}^3/\text{g}$. ICP-SFMS was used for elemental analysis and it was found that the Si to Al ratio was 3.56 and the Cu loading 3.1 wt%, resulting in an exchange level of 0.16Cu/Al; the SSZ-13 is thus under-exchanged. Further, 1.57 wt% sodium was present from the synthesis, in addition to small amounts of iron (0.06 wt%).

4.2. Kinetic model for ammonia storage and release by combining micro-calorimetry and flow reactor experiments

We have previously developed a method for determining the coverage dependent heat of adsorption at atmospheric pressure and applied this technique to ammonia storage over Cu/BEA [41]. In the setup, the catalyst powder was placed on a sintered quartz plate

in a quartz reactor and the sample was thereafter exposed to gas containing ammonia. Since ammonia adsorbs very easily, it preferentially adsorbs in the initial part of the bed and thereafter further down the bed, like a plug flow reactor. The reaction heat that we measure is an average of both strongly and loosely bound ammonia. We therefore, start to adsorb ammonia at a high temperature, where only the most strongly bound ammonia is attached, resulting in a high heat of adsorption. Thereafter, the temperature was decreased, while exposing the catalyst to inert Ar. When the next set point of temperature was reached, ammonia was again dosed over the sample and this time, ammonia that is less strongly bound gets adsorbed. This procedure was repeated, with lower and lower temperature, and was used to determine ΔH as a function of coverage. The result was a linear function [41], in accordance with the Temkin isotherm. The resulting coverage dependent heat of adsorption [56] was successfully used in a kinetic model for hydrothermal aging of Cu/zeolites used for ammonia-SCR [36].

In this paper, we have applied the above technique to ammonia adsorption over Cu/SSZ-13 using a broad temperature interval, starting at 500°C and stepwise decreasing the temperature by 50°C steps to 50°C . For noble metal catalysts, for example, the number of sites can be determined by measuring the dispersion. However, this approach cannot be used to determine the number of sites for ammonia adsorption on Cu/zeolites. The lower the temperature, the more ammonia gets adsorbed [33]. Accordingly, a temperature must be chosen where the number of sites can be determined based on the amount of ammonia storage. In the first simulations in this study, we chose 50°C since it is the lowest temperature in our experiments. With this assumption, it is possible to calculate the ammonia coverage as a function of the ΔH , where the ΔH is the highest at the adsorption temperature of 500°C , and decreases to reach the lowest value for adsorption at a temperature of 50°C . The resulting heat of adsorption versus NH_3 coverage is shown in Fig. 1a. A straight line fit is made resulting in the following activation energy for ammonia desorption (assuming the adsorption is non-activated):

$$E_{\text{NH}_3, \text{desorption}} = 163.39 (1 - 0.596 \cdot \theta_{\text{S1-NH}_3}) \text{ kJ/mol} \quad (7)$$

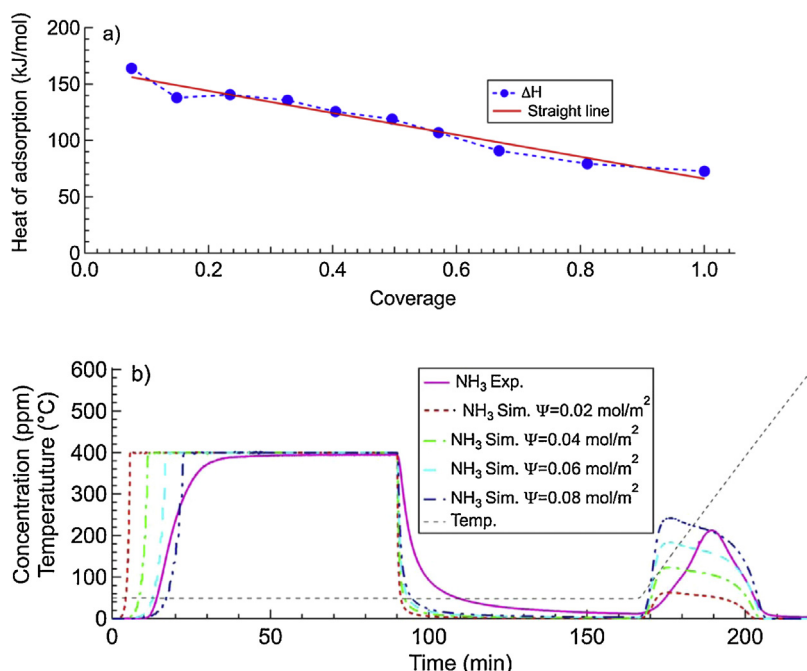


Fig. 1. (a) The heat of adsorption versus coverage for ammonia adsorption on Cu/SSZ-13. (b) Experiment and kinetic model for NH_3 TPD, using different site densities and Reaction (1), Table 1.

This barrier was used to simulate an ammonia TPD experiment conducted in the flow reactor using a monolith. In the experiment, the catalyst was exposed to 400 ppm NH₃ and 5% H₂O at 50 °C and after 90 min, the catalyst was flushed with 5% H₂O in Ar and thereafter, the temperature was increased to 600 °C. The results from this experiment are shown in Fig. 1b. In addition, the results from a kinetic model using only one reaction step for ammonia adsorption and desorption, according to Reaction (1) in Table 1, are shown. In this simulation, the coverage dependent activation energy for ammonia desorption (Eq. (7)) was used and the site density was varied. It is clear from the simulations that when changing the site density, the prediction of the ammonia adsorption is improved; however, the ammonia desorption peak is much too broad and do not either explain the loosely bound ammonia desorbing when flushing the catalyst with inert feed at 50 °C. This method worked well for the previous simulations on Cu/BEA. In the earlier simulations, the model was valid from 150 °C, whereas in this study, temperatures as low as 50 °C were simulated. At such low temperatures, large amounts of physisorbed ammonia are also present and a multiple storage site model must be used.

The results from the simulations in Fig. 1b indicate that at least two storage sites are needed in the model, the main S1 site and another site for loosely bound physisorbed ammonia. In order to further examine the desorption behavior, the ammonia concentration versus desorption temperature is shown in Fig. 2a. A main desorption peak is observed with a maximum peak at about 285 °C; in addition, shoulders are observed at both low and high temperature. Further, the simulations of ammonia oxidation and SCR, which will be discussed in later sections, show that two active sites are needed to simulate the activity over a broad temperature interval (100–600 °C). In addition, over both Cu/BEA [22] and Cu/SSZ-13 [23], it has been suggested that the oxidation and SCR reactions occur on different types of copper species. Based on these results, we develop a model with three storage sites, which is described in Sections 3.2 and 4.3. Briefly it consists of S1, S2 and S3, where S1 represents copper in the six-membered ring and S2 copper in the large cages. In addition, ammonia is also

stored on Brønsted acid sites, but in order not to complicate the model further, it was lumped together in the S1 and S2 sites. In several previous studies the ammonia storage has been lumped together successfully [12,31,36,44,52,53]. Finally, S3 is a site for physisorption that occurs at low temperature. The physical interpretation of the sites will be more thoroughly discussed in Section 4.3.

Based on this three-site model, the micro-calorimeter data were divided into three regions; a low temperature region, another region at medium temperatures and a third region at high temperatures. The main storage site, S1, was first studied and different temperatures from the micro-calorimeter data were tried and incorporated into the kinetic model. We found that the best agreement with the TPD results in the monolith was obtained when we used the micro-calorimeter data from 250 to 400 °C, which are shown in Fig. 2b. This resulted in the following activation energy for ammonia desorption:

$$E_{\text{NH}_3, \text{desorption}} = 149.0 (1 - 0.20 \cdot \theta_{\text{S1-NH}_3}) \text{ kJ/mol} \quad (8)$$

When comparing this expression with the previous one (Eq. (7)), it becomes clear that the coverage dependence is much lower now, 0.20 compared to 0.596. The results in Fig. 1b show a too broad TPD peak because of high coverage dependence in the model, and it is therefore, beneficial that the updated coverage dependence is much lower.

The reactions and rate expressions for the ammonia storage on these three sites are shown in Reactions (1)–(3) in Table 1. First, the ammonia storage on only S1 is simulated, using the activation energy for ammonia desorption according to Eq. (8), and the resulting simulation together with experiment is shown in Fig. 3. The model is now capable of describing the main ammonia desorption peak well. It has become clear that a large amount of physisorbed ammonia is needed for low temperature storage which will be added to the model through adsorption on S3. In addition, the model is under-predicting the ammonia desorption at the highest temperature which will be simulated by ammonia storage on S2.

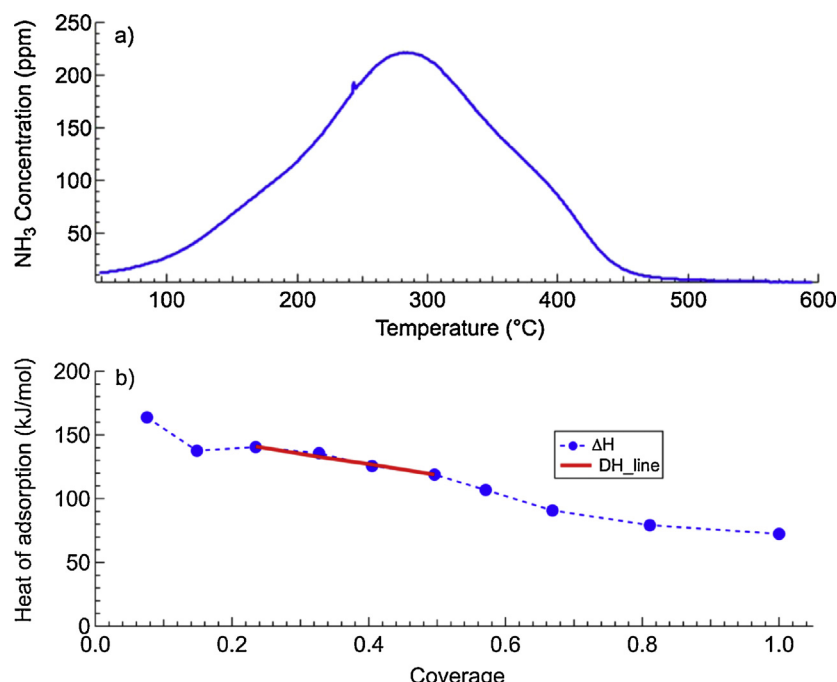


Fig. 2. (a) Ammonia concentration during temperature ramp in TPD. (b) The heat of adsorption versus coverage for ammonia adsorption on Cu/SSZ-13. Straight line fit for main storage site.

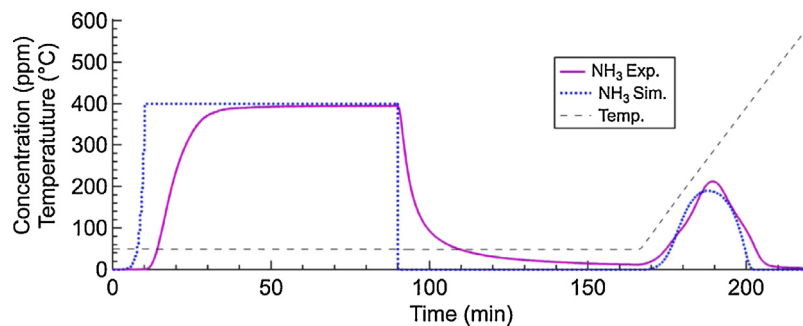


Fig. 3. Experiment and kinetic model for NH_3 TPD at 50°C using Reaction (1), Table 1, and activation energy from Eq. (8).

The next step in the model development was to add the ammonia storage on S2 and S3. For the storage of ammonia at high temperature on S2, the ΔH from the micro-calorimeter measurement at 450°C was used (see Fig. 2b) since only a minor amount of ammonia was desorbed at 500°C (see Fig. 2a), the highest temperature in the calorimeter experiments. This resulted in an activation energy for ammonia desorption of 137.8 kJ/mol . For the S3 site, a corresponding heat of adsorption at 50°C was used, which resulted in an activation energy for ammonia desorption of 72.6 kJ/mol . The results from using these three reactions and tuning the values for pre-exponential factors and site densities for S2 and S3 to simulate the NH_3 TPD at 50°C are shown in Fig. 4a. The model is capable of describing the experimental features adequately. The model has somewhat too sharp profile at the end of the adsorption compared to the simulation, but the amount of ammonia stored close to saturation is only a minor part of the total storage. Using the same model and parameters, a corresponding TPD conducted at 150°C was simulated, with the results shown in Fig. 4b. The model is not capable of predicting the loosely bound ammonia desorbing when turning ammonia off at 150°C and in addition, too much ammonia is released in the model during the early phase of the temperature ramp. Further, the total storage of ammonia is under-predicted by the model.

Since the agreement of the model shown in Fig. 4 was unsatisfactory, further development is needed. The simulations at medium and high temperatures well agree with the experiments for both 50 and 150°C TPD. Therefore, the parameters for S1 and S2 remain and the parameters for S3 are instead changed. In the simulations in Fig. 4, the ΔH for 50°C was used and we now instead use ΔH for the 150°C point in the micro-calorimeter experiment, which was 90.8 kJ/mol . The resulting simulation for the TPD at 150°C is shown in Fig. 5a and there is good agreement between model and simulation. However, when this model is applied to the TPD at 50°C (Fig. 5b), severe discrepancy between model and experimental data were observed. The model predicts no ammonia desorption when ammonia is turned off, but rather a huge desorption peak when the temperature is increased because the activation energy for ammonia desorption is much too high, resulting in ammonia desorption at too high a temperature.

The simulations have illustrated that it is difficult to use the micro-calorimeter experiments to determine the ΔH for the physisorbed ammonia. The reason for this difficulty is that the physisorbed ammonia is very dependent on the temperature and is not well defined. It likely incorporates a complex storage mechanism with adsorption on different sites. In addition, it is possible that the storage of several ammonia molecules on each site might be

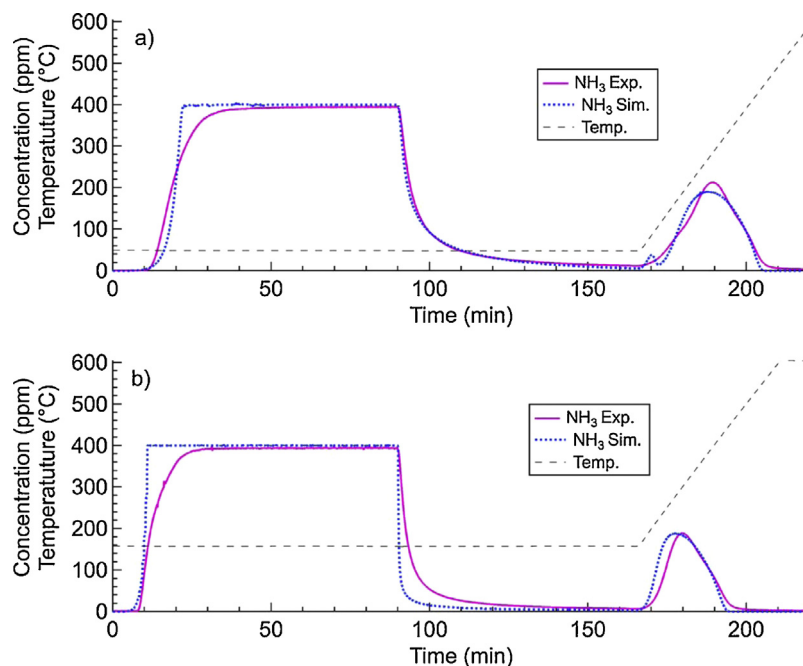


Fig. 4. Experiment and kinetic model for NH_3 TPD using Reactions (1)–(3), Table 1, and activation energy from ammonia desorption for S1: from Eq. (8), S2: 137.8 kJ/mol and S3: 72.6 kJ/mol . (a) TPD from at 50°C and (b) TPD from 150°C .

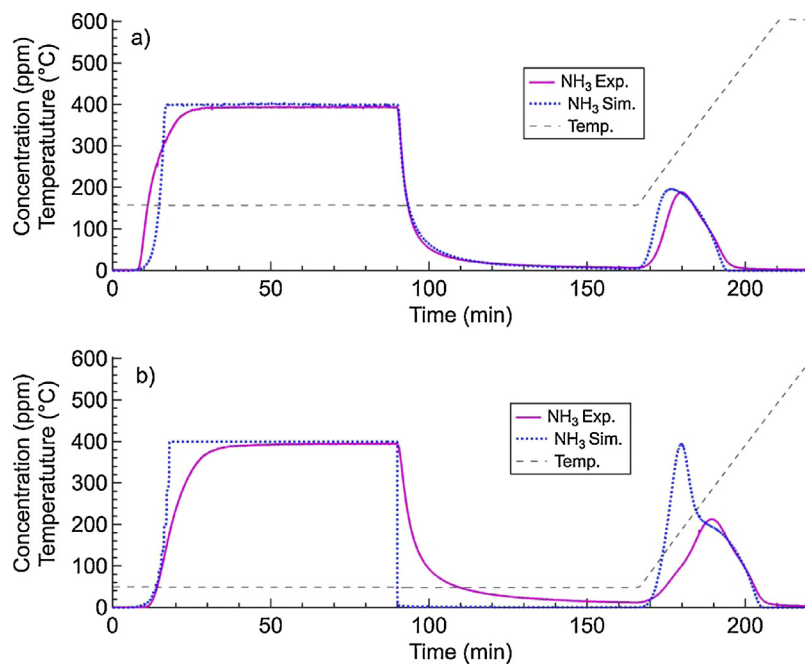


Fig. 5. Experiment and kinetic model for NH_3 TPD using Reactions (1)–(3), Table 1, and activation energy from ammonia desorption for S1: from Eq. (8), S2: 137.8 kJ/mol and S3: 90.8 kJ/mol. (a) TPD from at 150 °C and (b) TPD from 50 °C.

more important when reaching very low temperatures. Therefore, we have instead tried to tune the activation energy for ammonia desorption on S3 to the experimental results of the TPD at 50 and 150 °C, respectively. The outcome was an activation energy of 18.6 kJ/mol with the results for both the TPD at 50 and 150 °C depicted in Fig. 6. The model is now capable of well describing both the storage, including the slow adsorption close to saturation, as well as desorption for both the TPD at 50 and 150 °C. The parameters for the ammonia storage at S1, S2 and S3 are found in Table 2. The tuned site densities are 81.1, 7.84 and $1.29 \times 10^2 \text{ mol}/(\text{m}^3 \text{ monolith})$. The values for the activation energy for ammonia desorption

at zero coverage ($E_{A,i}^0$) is slightly higher for S1 compared to S2. However, since the activation energy ($E_{A,i}$) for desorption from S1 is coverage dependent which is no the case for S2, $E_{A,i}$ for coverages larger than 0.38 is smaller on S1 compared to S2. This is the reason for that the ammonia desorption occurs at a lower temperature on S1. In this study, we received a coverage dependence for the ammonia desorption from S1 of 0.2. In literature the values for coverage dependence are varying significantly and one of the reasons for this is if the model is a single site model or multiple sites model. If only one adsorption site is used the coverage dependence needs to be high in order to describe the temperature interval. For

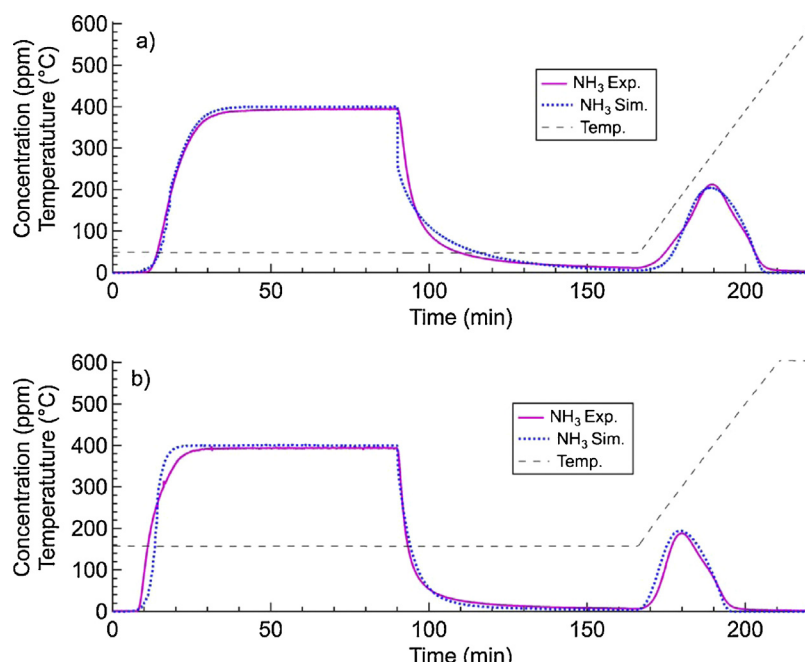


Fig. 6. Experiment and kinetic model for NH_3 TPD using Reactions (1)–(3), Table 1, and activation energy from ammonia desorption for S1: from Eq. (8), S2: 137.8 kJ/mol and S3: 18.6 kJ/mol. (a) TPD from at 50 °C and (b) TPD from 150 °C. All parameters are shown in Table 2.

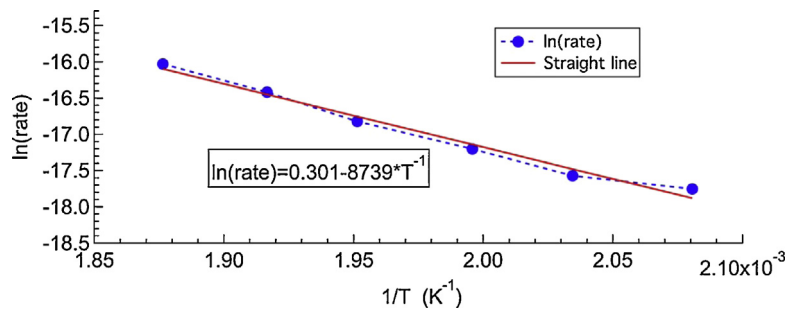


Fig. 7. Arrhenius plot for ammonia oxidation from 207.5 to 259.8 °C giving conversions from 1.8 to 10.1%.

example, Olsson et al. [36] used 0.39 in a kinetic model for ammonia desorption from Cu/BEA using a single site model. In a detailed multiple site model for Cu/ZSM-5, 0.133 was received for ammonia on the active copper site [33], which is a value more close to the one obtained in the present study.

4.3. Kinetic model for ammonia oxidation

An experiment dedicated to determining activation energies using Arrhenius plots was conducted for ammonia oxidation. In this experiment, the catalyst was exposed to 400 ppm NH₃, 8% O₂ and 5% H₂O and the temperature was stepwise increased by 10 °C intervals. The resulting Arrhenius plot from 207.5 to 259.8 °C (catalyst temperature), corresponding to conversions of between 1.8 and 10.1%, is shown in Fig. 7. The resulting activation energy was 72.7 kJ/mol, a value lower than expected that will be further discussed in the context of the model.

The experimental results of an ammonia oxidation experiment involving 400 ppm NH₃, 8% O₂ and 5% H₂O from 150 to 600 °C is shown in Fig. 8. The ammonia oxidation started with a low rate at 250 °C and slowly increased with temperatures to 350 °C. Interestingly, at 400 °C the ammonia conversion was slightly lower than at 350 °C. Thereafter, the ammonia oxidation was again increased at 500 and 600 °C. This behavior cannot be explained by a single Arrhenius reaction step. Therefore, we propose that there are two types of copper species and that the ammonia oxidation occurs

on them with different rates. These results are in line with the study by Gao et al. [29], who observed different activation energies for ammonia oxidation at high and low temperature. In an earlier study, we observed that the reaction rate for ammonia and NO oxidation over Cu/BEA was higher for over-exchanged sites, whereas for ammonia-SCR the rate was lower for the over-exchanged sites [22]. The reactions likely occurred on both types of sites, but the rates were faster for the different reactions on the two sites. With these results as a base, we developed a kinetic model for aging into which we incorporated two aging factors, one for under-exchanged sites, where SCR was dominating, and another for over-exchanged sites where oxidation reactions were preferred [36]. For Cu/SSZ-13, ammonia is believed to be initially ion-exchanged into isolated positions in the six-membered rings [26–28], probably slightly distorted due to the interaction with water and ammonia [26,29]. For higher copper loadings, it was suggested that copper was either occupying sites in the large cages [29,30] or forming Cu_xO_y species [28]. Bates et al. [28] studied Cu/SSZ-13 (Si/Al ~ 4.3–4.5) and found that below Cu/Al of 0.20, the copper was situated in the six-membered ring and concluded that this copper species was inactive for NO oxidation and a zero NO oxidation rate for Cu/Al of 0.2 and below [23] was observed. In our Cu/SSZ-13 sample, the Cu/Al ratio is 0.16, which is slightly lower than the 0.2 level that Bates et al. [28] reported. However, our catalyst has NO oxidation activity, which the lower loading samples from Bates et al. [28] did not possess. We observe the formation of 20–25 ppm NO₂ at 500–600 °C when

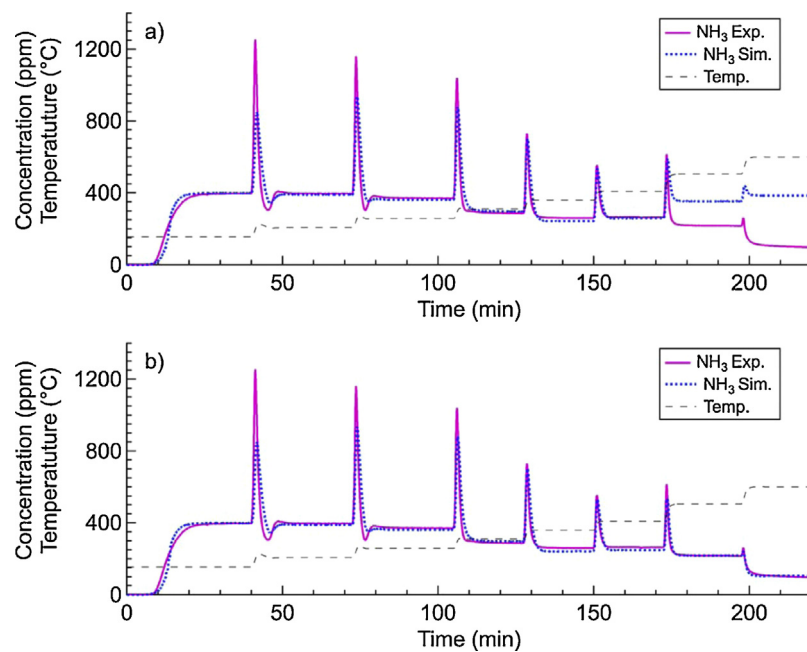


Fig. 8. Experiment and kinetic model for ammonia oxidation using (a) Reactions (1)–(4), Table 1, and (b) Reaction (1)–(5), Table 1.

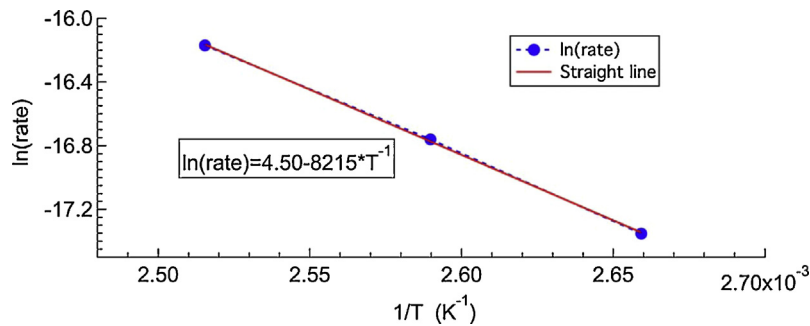


Fig. 9. Arrhenius plot for ammonia-SCR from 102.9 to 124.4 °C giving conversions from 2.7 to 8.8%.

exposing the catalyst to 400 ppm NO, 8% O₂ and 5% H₂O (results not shown here). Based on these findings, we suggest that our Cu/SSZ-13 sample primarily contains copper located in the six membered ring, in addition to some copper in the larger cages or in the form of Cu_xO_y species.

In the model, the copper sites in the six-membered rings are represented by S1, whereas the sites exchanged in either the cages or in Cu_xO_y form is represented by S2. As previously described, the ammonia storage on the Brönsted acid sites are included in the S1 and S2 sites in order not to further complicate the model. Combining the storage of ammonia on Brönsted sites and active copper sites into one site has been successfully performed in many previous kinetic models [12,31,36,44,52,53]. In accordance with the study by Bates et al. [28], we propose that the main SCR reaction occurs on the S1 sites. In addition, we suggest that the primary ammonia oxidation occurs on S2 sites similarly as was done in our aging model [36]. However, for ammonia oxidation, we observed a slow oxidation at low temperature and a more rapid increase at higher temperature. Since the experiments used for the Arrhenius plot were conducted at low temperature, the barrier received was associated with NH₃ oxidation at low temperature. For many Cu/zeolites, such as Cu/BEA and CuZSM-5, ammonia oxidation was mostly occurring at high temperature and accordingly, we suggest that the high temperature ammonia oxidation was related to the S2 sites and the low temperature oxidation was related to the S1

sites. Based on this mechanistic interpretation, we added a reaction step for ammonia oxidation occurring on S1 (Reaction (4), Table 1), with an activation barrier of 72.7 kJ/mol from the Arrhenius plot (Fig. 7) and the pre-exponential factor tuned (see Table 2 for parameters). The reaction rate is found in Table 1, and the reaction order of oxygen was found using multiple oxygen concentrations in simulations of ammonia oxidation over Cu/BEA (results not shown here). The outcome of this simulation is shown in Fig. 8. The model well described the ammonia oxidation from 150 to 400 °C, whereas it significantly under-predicted the ammonia oxidation at high temperature. The reason for this under-prediction is that at higher temperature, the coverage of ammonia on S1 was very low, which is seen in Fig. 3, where the simulation of ammonia desorbing from only S1 sites is depicted. Since the ammonia oxidation occurred with ammonia adsorbed on the surface, the ammonia oxidation rate went down when the coverage was decreased. On S2, on the other hand, the ammonia is bond more strongly at high temperature, which facilitates reactions at high temperature. Note that, the reason for the decrease in ammonia concentration directly after the ammonia desorption peak was that the temperature was increasing slightly above the set point and was thereafter decreasing again. The decrease in temperature resulted in an increased ammonia storage, which caused a dip in ammonia concentration.

In the next simulation, the main ammonia oxidation step on S2 was added (see Reaction (5), Table 1) and the activation energy was

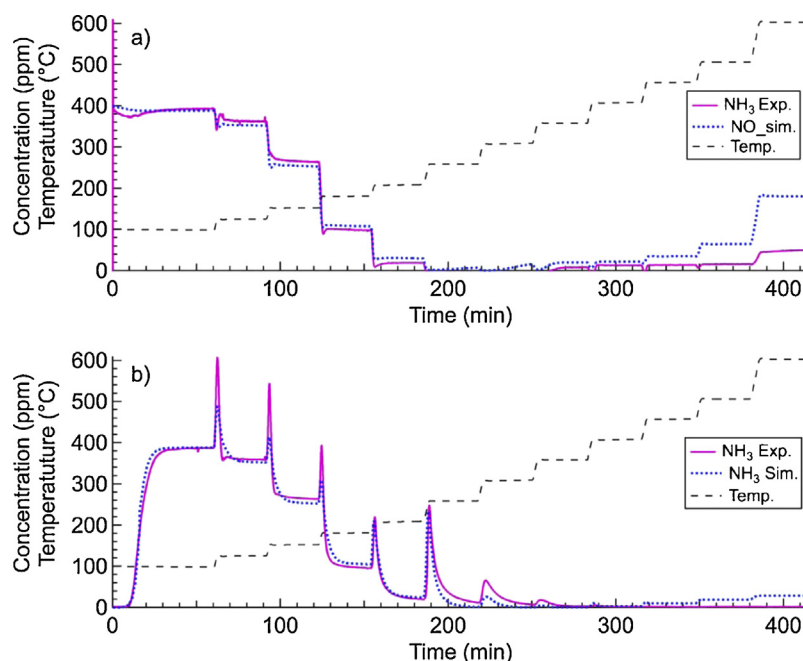


Fig. 10. Experiment and kinetic model for ammonia-SCR using Reactions (1)–(6), Table 1, where (a) shows the NO concentration and (b) the ammonia concentration.

tuned, resulting in an activation energy of 195.0 kJ/mol. This value is similar to what has been found in other modeling studies, for example 162.4 kJ/mol for Cu/ZSM-5 [31], 178.8 kJ/mol for Cu/CHA [37] and 180.0 kJ/mol for Cu/BEA [36]. The results from the updated model, including ammonia oxidation on both S1 and S2, are shown in Fig. 8b. The model describes the experimental findings very well. Using the findings from the modeling, we now propose a mechanism for the surprising features of the ammonia oxidation, where the conversion is slightly decreasing between 350 and 400 °C. At low temperature, ammonia oxidation occurs at a low rate on S1. When increasing the temperature, the ammonia coverage on S1 is decreased, which results in a decreased ammonia oxidation rate and this is the reason for the decrease in conversion between 350 and 400 °C. Further, when the temperature is increased to higher temperatures (500 and 600 °C), ammonia oxidation on S2 starts to occur, which results in a higher ammonia conversion.

4.4. Kinetic model for ammonia-SCR, including N_2O formation

Using the same approach as for ammonia oxidation, a special experiment was conducted for receiving data that could be used for an Arrhenius plot for ammonia-SCR. The catalyst was exposed to 400 ppm NH_3 , 400 ppm NO, 8% O_2 and 5% H_2O and increasing the temperature stepwise, in steps of 10 °C. The resulting Arrhenius plot from 102.9 to 124.4 °C (catalyst temperature), with

corresponding conversions from 2.7 to 8.8%, is shown in Fig. 9. This resulted in an activation energy of 68.3 kJ/mol.

An ammonia-SCR experiment from 100 to 600 °C, using 400 ppm NH_3 , 400 ppm NO, 8% O_2 and 5% H_2O , was used to develop the model. One reaction was added for ammonia-SCR on S1 (Reaction (6), Table 1). The reaction order for oxygen in this reaction (Table 1) was previously determined using experiments containing several oxygen concentrations over Cu/BEA and the activation energy from the Arrhenius plot. The resulting NO and NH_3 concentration from the model and simulation is shown in Fig. 10. The ammonia-SCR is well-described up to 400 °C, but at higher temperatures both the NO and ammonia conversion is too low. The reason for the low conversion is that the coverage of ammonia at higher temperatures is too low on S1, resulting in a decrease of the overall rate, even though the rate constant is increasing due to the temperature. This outcome is in line with earlier simulations on Fe/zeolites conducted by Sjövall et al. [17], where an additional SCR step was needed to describe the high temperature SCR reaction. The results from the simulations in this study (see Fig. 10) clearly show that an SCR reaction on S1 is not sufficient to describe the SCR activity across the entire temperature interval.

For Cu/BEA, we earlier proposed that the SCR reaction is faster on the under- and medium-exchanged copper sites, but that the SCR reaction is also occurring on the over-exchanged sites albeit at lower rates [22]. Our simulation results in this study also indi-

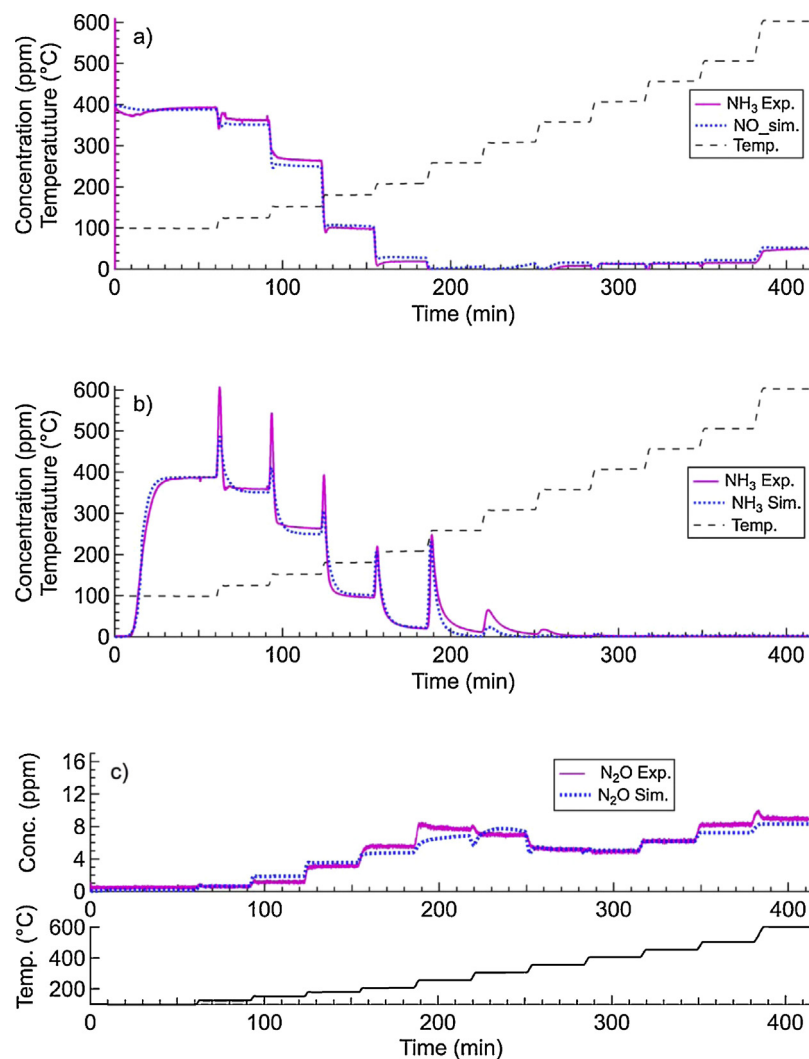


Fig. 11. Experiment and kinetic model for ammonia-SCR using Reactions (1)–(10), Table 1, where (a) shows the NO concentration, (b) NH_3 and (c) N_2O concentrations.

cated that this was also the case for Cu/SSZ-13. We therefore added a reaction step for ammonia-SCR on S2, which occurred only at the highest temperatures (see Reaction (7), **Table 1**). In addition, we have observed the complex behavior for the N₂O formation for Cu/SSZ-13, similar to Cu/BEA [36,57], where the N₂O formation exhibited a maximum at 250 °C, followed by a decrease in N₂O production; however, from 450 °C it started to increase again. In addition, we found that after thermal aging, the N₂O formation at low temperature decreased, whereas the N₂O production at high temperature increased. It is therefore likely that there are two different mechanisms for the N₂O formation, which we included in a kinetic model for N₂O formation during SCR conditions over Cu/BEA [36]. The N₂O formation at low temperature is often suggested to be connected to the ammonium nitrate formation [22,57]. We therefore added the formation of ammonium nitrate precursors into the model [36] and it is crucial that this formation was reversible (Reaction (8), **Table 1**) in order to describe the maximum N₂O production. The precursors can react to form N₂O, which is done in Reaction (9) (**Table 1**). Thus, when the temperature was increased, the ammonium nitrate precursor was decomposed and its coverage thereby decreased. This process will result in decreased N₂O formation leading to the maximum N₂O production at low temperature. This mechanism is in accordance with the study performed by Colombo et al. [44], where S-NO₃[NH₃] was used in the detailed mechanism for N₂O formation over commercial Cu/zeolites. As described above, the N₂O formation started to increase again at high temperature which is why an additional reaction step was added [36], as seen in Reacion (10), **Table 1**.

The updated mechanism, including the SCR reaction on S1 and S2 and the N₂O reaction steps, was used to simulate the SCR experiment from 100 to 600 °C, with the results shown in **Fig. 11**. The updated model well describes the NO, NH₃ and N₂O concentrations. All reactions, rates and their corresponding parameters are given in **Tables 1 and 2**, respectively.

5. Conclusions

In this study, we have developed a kinetic model for ammonia-SCR over a well-characterized Cu/SSZ-13 catalyst. Based on flow reactor data, both ammonia oxidation and NH₃-SCR activity, as well as ammonia storage and release data, we propose a three-site model. Previous studies, when varying the copper loading, has suggested that over both Cu/BEA as well as Cu/SSZ-13 there are two active copper sites; where the SCR reaction occurs mainly on the under-exchanged sites and the oxidation reactions on the over-exchanged sites. Using these results as a base we have introduced two sites, S1 and S2, in order to represent these two active copper species. Ammonia is also known to store on the Brønsted acid sites, but in order not to further complicate the model, the storage on Brønsted sites was lumped into the S1 and S2 sites, which is an approach that have been done successfully in many other studies.

In studies available in the literature, where Cu/SSZ-13 have been thoroughly characterized using many different experimental techniques, it was concluded that for low copper loading, copper was located in the six-membered ring, possibly slightly distorted due to interactions with ammonia and water. Since our sample had a low ion-exchange level, it was likely that a large portion of the copper is inside the six-membered ring, denoted as S1 in the model. When modeling the ammonia TPD experiments, the NH₃ on the S1 site is responsible for the main ammonia desorption peak, with a maximum at 285 °C. Further, the S2 sites were used for modeling the high temperature shoulder in the ammonia TPD. In the literature, it is proposed that after the copper exchange inside the six-membered ring, the exchange starts to occur inside the large cage or by possibly forming Cu_xO_y species. These species are suggested to be responsi-

ble for the NO oxidation, and with our Cu/SSZ-13, we observed some NO₂ formation during NO oxidation. We therefore suggest that the physical interpretation of the copper species associated with S2 sites is copper located inside the large cages or Cu_xO_y species. In addition, the ammonia TPD, using 50 °C as adsorption temperature, showed large amounts of physisorbed ammonia as described in the model by adding a third site, S3. The model using these three storage sites could well describe the ammonia TPD experiments, with storage at 50 and 150 °C, respectively. In the model, the heat of adsorption of ammonia on S1 and S2 was determined using separate micro-calorimeter experiments.

In the literature, it has been suggested that ammonia-SCR primarily occurs on copper sites in the six-membered ring and that NO oxidation is occurring on copper sites at higher exchange levels. Based on these results, we have developed a mechanism whereby the main SCR reaction is occurring on S1 and the main ammonia oxidation reaction on S2. Ammonia oxidation on the Cu/SSZ-13 showed an interesting behavior by which the ammonia conversion was slightly decreased at 400 °C compared to 350 °C. In the model, it was therefore crucial to add ammonia oxidation reactions to both S1 and S2, where the ammonia oxidation on S2 was the primary reaction occurring at higher temperature. The model could well describe the experimental features by the following mechanism. At low temperature, ammonia oxidation occurred at a low rate on S1, with the activation energy for this reaction determined from Arrhenius plots at low temperature. When the temperature was increased, the coverage of ammonia on the S1 sites was significantly decreased. Since the reaction rate for ammonia oxidation is proportional to the ammonia coverage, a decreased rate and thereby decreased conversion followed. At higher temperatures, the ammonia oxidation on S2 started and a higher conversion was then received.

As mentioned above, the main ammonia-SCR reaction occurred on S1, but this was not sufficient in order to describe the entire temperature interval (100–600 °C). The model could well predict the SCR reaction up to 400 °C, but at higher temperatures, the conversion in the model was too low because the coverage of ammonia on S1 was also too low. We therefore, introduced ammonia-SCR also on S2, which stores ammonia at higher temperatures. The updated mechanism could well describe the NO and ammonia concentrations across the entire temperature interval. In addition, the N₂O formation possessed a very complex behavior, on Cu/SSZ-13, which we have previously observed on Cu/BEA. The N₂O formation exhibited a maximum at low temperature and in addition, the production again increased at high temperature. We used the N₂O mechanism previously developed for Cu/BEA in order to simulate the N₂O production during standard SCR conditions. To summarize, when using the full model including the N₂O mechanism, the model was capable of describing all experimental features for NO, NH₃ and N₂O across the entire temperature interval (100–600 °C).

Acknowledgments

This study was performed by Chemical Engineering and the Competence Centre for Catalysis at Chalmers University and Cummins Inc. The financial support of Cummins Inc. and the Swedish Research Council (621-2011-4860) are gratefully acknowledged.

References

- [1] I. Nova, L. Lietti, E. Tronconi, P. Forzatti, *Chem. Eng. Sci.* 56 (2001) 1229–1237.
- [2] B. Roduit, A. Wokaun, A. Baiker, *Ind. Eng. Chem. Res.* 37 (1998) 4577–4590.
- [3] J.A. Dumesic, N.-Y. Topsoe, H. Topsoe, Y. Chen, T. Slabiak, *J. Catal.* 163 (1996) 409–417.
- [4] L. Lietti, I. Nova, E. Tronconi, P. Forzatti, *Catal. Today* 45 (1998).
- [5] D. Chatterjee, T. Burkhardt, M. Weibel, E. Tronconi, I. Nova, C. Ciardelli, *SAE 2006-01-0468* (2006).

[6] H. Sjövall, L. Olsson, E. Fridell, R.J. Blint, *Appl. Catal. B* 64 (2006) 180.

[7] H. Sjövall, E. Fridell, R.J. Blint, L. Olsson, *Top. Catal.* 42–43 (2007) 113–117.

[8] J.-H. Park, H.J. Park, J.H. Baik, I.-S. Nam, C.-H. Shin, J.-H. Lee, B.K. Cho, S.H. Oh, *J. Catal.* 240 (2006) 47–57.

[9] S. Kieger, G. Delahay, B. Coq, B. Neveu, *J. Catal.* 183 (1999) 267–280.

[10] J.A. Sullivan, J. Cunningham, M.A. Morris, K. Keneavey, *Appl. Catal. B: Environ.* 7 (1995) 137–151.

[11] K. Rahkamaa-Tolonen, T. Maunula, M. Lomma, M. Huuhtanen, R.L. Keiski, *Catal. Today* 100 (2005) 217–222.

[12] A. Pant, S.J. Schmieg, *Ind. Eng. Chem. Res.* 50 (2011) 5490–5498.

[13] A. Grossale, I. Nova, E. Tronconi, D. Chatterjee, M. Weibel, *Top. Catal.* 52 (2009) 1837–1841.

[14] P.S. Metkar, V. Balakotaiah, M.P. Harold, *Catal. Today* 184 (2012) 115–128.

[15] S. Malmberg, M. Votsmeier, J. Gieshoff, N. Söger, L. Mußmann, A. Schuler, A. Drochner, *Top. Catal.* 42–43 (2007) 33–36.

[16] D. Chatterjee, T. Burkhardt, M. Weibel, I. Nova, A. Grossale, E. Tronconi, *SAE 2007-01-1136* (2007).

[17] H. Sjövall, R.J. Blint, A. Gopinath, L. Olsson, *Ind. Eng. Chem. Res.* 49 (2010) 39–52.

[18] K. Kamasamudram, N.W. Currier, X. Chen, A. Yezersets, *Catal. Today* 151 (2010) 212–222.

[19] L. Wang, W. Li, G.S. Qi, D. Weng, *J. Catal.* 289 (2012) 21–29.

[20] S.J. Schmieg, S.H. Oh, C.H. Kim, D.B. Brown, J.H. Lee, C.H.F. Peden, D.H. Kim, *Catal. Today* 184 (2012) 252–261.

[21] D.W. Fickel, E. D'Addio, J.A. Lauterbach, R.F. Lobo, *Appl. Catal. B Environ.* 102 (2011) 441–448.

[22] O. Mihai, C. Widjastuti, S. Andonova, K. Kamasamudram, J. Li, S. Joshi, N.W. Currier, A. Yezersets, L. Olsson, *J. Catal.* 311 (2014) 170.

[23] A.A. Verma, S.A. Bates, T. Anggara, C. Paolucci, A.A. Parekh, K. Kamasamudram, A. Yezersets, J.T. Miller, W.N. Delgass, W.F. Schneider, F.H. Ribeiro, *J. Catal.* 312 (2014) 179–190.

[24] J.S. McEwen, T. Anggara, W.F. Schneider, V.F. Kispersky, J.T. Miller, W.N. Delgass, F.H. Ribeiro, *Catal. Today* 184 (2012) 129–144.

[25] J.H. Kwak, D. Tran, J. Szanyi, C.H.F. Peden, J.H. Lee, *Catal. Lett.* 142 (2012) 295–301.

[26] U. Deka, A. Juhin, E.A. Eilertsen, H. Emerich, M.A. Green, S.T. Korhonen, B.M. Weckhuysen, A.M. Beale, *J. Phys. Chem. C* 116 (2012) 4809–4818.

[27] D.W. Fickel, J.M. Fedeyko, R.F. Lobo, *J. Phys. Chem. C* 114 (2010) 1633–1640.

[28] S.A. Bates, A.A. Verma, C. Paolucci, A.A. Parekh, T. Anggara, A. Yezersets, W.F. Schneider, J.T. Miller, W.N. Delgass, F.H. Ribeiro, *J. Catal.* 312 (2014) 87–97.

[29] F. Gao, E.D. Walter, E.M. Karp, J.Y. Luo, R.G. Tonkyn, J.H. Kwak, J. Szanyi, C.H.F. Peden, *J. Catal.* 300 (2013) 20–29.

[30] J.H. Kwak, H.Y. Zhu, J.H. Lee, C.H.F. Peden, J. Szanyi, *Chem. Commun.* 48 (2012) 4758–4760.

[31] L. Olsson, H. Sjövall, R.J. Blint, *Appl. Catal. B* 81 (2008) 203–217.

[32] L. Olsson, H. Sjövall, R.J. Blint, *Appl. Catal. B: Environ.* 87 (2009) 200.

[33] H. Sjövall, L. Olsson, R.J. Blint, *J. Phys. Chem. C* 113 (2009) 1393.

[34] H. Sjövall, R.J. Blint, L. Olsson, *Appl. Catal. B* 92 (2009) 138.

[35] G. Delahay, S. Kieger, N. Tanchoux, P. Trems, B. Coq, *Appl. Catal. B Environ.* 52 (2004) 251–257.

[36] K. Supriyanto, A. Wijayanti, S. Kumar, K. Joshi, N.W. Kamasamudram, A. Currier, L. Yezersets Olsson, *Appl. Catal. B Environ.* 163 (2015) 382.

[37] P.S. Metkar, M.P. Harold, V. Balakotaiah, *Chem. Eng. Sci.* 87 (2013) 51–66.

[38] S.A. Stevenson, J.C. Vartuli, C.F. Brooks, *J. Catal.* 190 (2000) 228–239.

[39] M. Colombo, I. Nova, E. Tronconi, V. Schmeisser, B. Bandl-Konrad, L. Zimmermann, *Appl. Catal. B Environ.* 111 (2012) 106–118.

[40] J.H. Baik, S.D. Yim, I.S. Nam, Y.S. Mok, J.H. Lee, B.K. Cho, S.H. Oh, *Ind. Eng. Chem. Res.* 45 (2006) 5258–5267.

[41] N. Wilken, K. Kamasamudram, N.W. Currier, J. Li, A. Yezersets, L. Olsson, *Catal. Today* 151 (2010) 237.

[42] M. Colombo, G. Koltzakis, I. Nova, E. Tronconi, *Catal. Today* 188 (2012) 42–52.

[43] S.A. Skarlis, D. Berthout, A. Nicolle, C. Dujardin, P. Granger, *J. Phys. Chem. C* 117 (2013) 7154–7169.

[44] M. Colombo, I. Nova, E. Tronconi, *Catal. Today* 197 (2012) 243–255.

[45] R. Nedjalkova, K. Kamasamudram, N.W. Currier, J. Li, A. Yezersets, L. Olsson, *J. Catal.* 299 (2013) 101.

[46] K. Wijayanti, S. Andonova, A. Kumar, J. Li, K. Kamasamudram, N.W. Currier, A. Yezersets, L. Olsson, *Appl. Catal. B: Environ.* 166–167 (2015) 568.

[47] AVL BOOST Aftertreatment Manual, AVL, (2009) <http://www.avl.com>

[48] D. Chatterjee, T. Burkhardt, B. Bandl-Konrad, T. Braun, E. Tronconi, I. Nova, C. Ciardelli, *SAE 2005-01-0965* (2005).

[49] M. Colombo, I. Nova, E. Tronconi, *Catal. Today* 151 (2010) 223–230.

[50] M. Boudart, G. Djega-Mariassou, *Kinetics of Heterogeneous Catalytic Reactions*, Princeton University Press, 1984.

[51] E. Tronconi, I. Nova, C. Ciardelli, D. Chatterjee, B. Bandl-Konrad, T. Burkhardt, *Catal. Today* 105 (2005) 529–536.

[52] I. Nova, D. Bounechada, R. Maestri, E. Tronconi, A.K. Heibel, T.A. Collins, T. Boger, *Ind. Eng. Chem. Res.* 50 (2011) 299–309.

[53] T.C. Watling, M.R. Ravenscroft, G. Avery, *Catal. Today* 188 (2012) 32.

[54] Q. Zhu, J.N. Kondo, T. Tatsumi, S. Inagaki, R. Ohnuma, Y. Kubota, Y. Shimodaira, H. Kobayashi, K. Domen, *J. Phys. Chem. C* 111 (2007) 5409–5415.

[55] T. Gunter, M. Casapu, D. Doronkin, S. Mangold, V. Trouillet, T. Augenstein, J.D. Grunwaldt, *Chem. Ing. Tech.* 85 (2013) 632–641.

[56] N. Wilken, K. Wijayanti, K. Kamasamudram, N.W. Currier, R. Vedaiyan, A. Yezersets, L. Olsson, *Appl. Catal. B* 111 (2012) 58.

[57] O. Mihai, C.R. Widjastuti, A. Kumar, J. Li, S.Y. Joshi, K. Kamasamudram, N.W. Currier, A. Yezersets, L. Olsson, *Catal. Lett.* 144 (1) (2014) 70.